The composition dependence of the electronic properties of CuHf and CuZr amorphous metals

1997 J. Phys.: Condens. Matter 9 8601

(http://iopscience.iop.org/0953-8984/9/41/007)

J. Phys.: Condens. Matter **9** (1997) 8601–8616. Printed in the UK PII: S0953-8984(97)83403-0

The composition dependence of the electronic properties of CuHf and CuZr amorphous metals

C G H Walker†‖, S A Morton†¶, P K Hucknall†, D Greig†, J A D Matthew†‡ and D Norman†§

† Department of Physics, University of Leeds, Leeds LS2 9JT, UK
‡ Department of Physics, The University of York, Heslington, York YO1 5DD, UK
§ Central Laboratory of the Research Councils, Daresbury Laboratory, Daresbury, Warrington WA4 4AD, UK

Received 14 April 1997, in final form 4 August 1997

Abstract. The nature of the electron state band in the amorphous metal alloys CuHf and CuZr has been studied using synchrotron radiation as a source in photoemission experiments. In the photon energy range $h\nu = 35$–45 eV the valence band undergoes resonant photoemission which emphasizes Hf 5d-like states in CuHf and Zr 4d-like states in CuZr, while at higher photon energies contributions from these states are strongly de-emphasized because of Cooper minima in their cross-sections. The ratio of the intensities of the valence band as compared with other peaks in the spectrum characteristic of Cu or Hf (Zr) shows that the near-Fermi-level region is not wholly Hf (Zr) d-like in character, but that the degree of hybridization of these states is less than in alloys such as FeZr where both elements have partially filled shells.

1. Introduction

The electrical conductivity of amorphous transition metal alloys has been of interest due to its anomalously low value which has been difficult to understand theoretically [1, 2]. Knowledge of the conduction band density of states would provide useful additional information required to interpret the transport properties of these materials. Photoemission provides the most direct way. Most previous x-ray and uv photo-emission experiments on these alloys [3–5] have not used synchrotron radiation. This provides the ability to tune the incident photons and thus be able to take advantage of the different photoemission cross-sections of various states as a function of photon energy, especially resonant enhancement and Cooper minima [6–8].

By the introduction of *in situ* magnetron sputtering techniques, the alloys have been deposited at a variety of compositions. The variation of the relative intensities of different peaks as a function of composition is shown to highlight hybridization in the amorphous state. This study extends preliminary work on CuHf and CuZr [8] through improved preparation techniques, systematic examination of concentration dependence and exploitation of the Cooper minima in the Hf 5d and Zr 4d cross-sections.

‖ Present address: Department of Applied Biological and Chemical Sciences, University of Ulster, Coleraine, County Londonderry, Northern Ireland BT52 1SA, UK.
¶ Present address: Chemistry Department, University of York, Heslington, York YO1 5DD, UK.

0953-8984/97/418601+16$19.50

2. Experimental details

The thin-film amorphous alloys were formed *in situ* by DC magnetron co-sputtering. The process was carried out in a UHV preparation chamber attached to the main experimental chamber. In this way samples could be transferred to the measurement position without breaking vacuum.

The magnetron targets were made from sheets of high-purity elemental materials. Research grade argon at a pressure of 3×10^{-3} mbar was used as the sputtering gas, which pumped away to leave a base pressure of 2×10^{-10} mbar in the chamber. The composition of the deposited film was controlled by regulating the power to each magnetron. Due to the geometry of the magnetron targets and the substrate, a small composition gradient ($\sim$1%) existed over the length of the specimen. This was anticipated and great care taken when positioning the sample for both UPS measurements and bulk analysis. Composition analysis of the samples was performed using AES at Daresbury, while bulk analysis was performed at Leeds using a Cameca Camebax SX50 electron microprobe. The amorphous character of the samples was confirmed by *in situ* resistivity measurement [9] which showed that the alloys retained the negative coefficient of resistivity that is characteristic of the amorphous state until either constituent reached approximately 80% of the total. *Ex situ* x-ray measurements on samples prepared in a commercial Edwards 320 sputtering system are consistent with such an amorphicity range.

The photoemission spectra were measured in a vacuum of 2×10^{-10} mbar on stations 6.1 and 6.2 of the Daresbury SRS; 6.2 covers an energy range of 15 eV to about 80 eV with a resolution measured directly from the tantalum Fermi edge of 0.25 eV at 15 eV to 0.5 eV at 80 eV, while in 6.1, 50 eV $< h\nu <$ 200 eV, the resolution is from approximately 0.4 to 0.8 eV. The spectra were collected with a double-pass angle integrating cylindrical mirror analyser (CMA) and have been normalized to the incident photon fluxes which were monitored continuously by measuring the drain currents from a tungsten grid positioned in the incoming beam.

3. Results

3.1. Estimates of atomic concentration

Two methods were used for the estimation of sample composition: (i) energy dispersive x-ray analysis (EDX), representative of the bulk; (ii) Auger analysis, representative of the surface, performed by measuring peak to peak heights of spectra displayed in the differential mode and comparing with published pure element standards [10]. The ratios of specimen Auger current to standard Auger current were corrected for matrix effects, electron backscattering, electron mean free path and atomic density using an iterative process [11]. The resulting composition estimates for some CuHf samples are shown in table 1. The CuHf analysis was performed using the 189 eV Hf MNN Auger peak of Hf. When the Hf LMM Auger peak at 1612 eV was used, better agreement with the EDX analysis was obtained, consistent with the 1612 eV Auger electrons having a longer mean free path than the 189 eV electrons. The differences between the results for the two analytic techniques are consistent with depth dependence in composition and a slight enhancement of Hf concentration at the surface. The mechanism by which this arises is not known in detail, but surface composition variations from the bulk after sputter deposition have been reported before in an entirely different system [12]. In comparing photoemission intensities as a function of composition Auger concentration estimates ignoring C and O contributions are used with the Cu and

Hf concentrations having an expected precision of a few per cent in the mid-concentration range and of the order of 1% in the low-Cu-concentration regime.

Table 1. Comparative estimated compositions of some CuHf samples using AES and EDX Auger analysis (EDX in brackets).

	I	II	III
Hf	34(21)	73(57)	85(76)
Cu	65(79)	24(43)	11(24)
C	0	1	2
O	1	2	2

3.2. CuHf photoemission—resonance region

UPS spectra from Cu_xHf_{1-x} normalized to photon flux were acquired in the photon energy range 25–60 eV (figure 1) for a variety of compositions. There are two peaks in the valence/conduction band region at 1 eV binding energy (peak A) and 3.5 eV (peak B) as in the outer electronic structure of CuTi: additional Hf 4f core photoemission (peak C) is observed in the range 14–16 eV. The Hf 4f signal builds up slowly with photon energy due to the delayed threshold associated with the high initial-state angular momentum: in contrast the intensity of peak A goes through a maximum in the photon energy range 40–50 eV. Figure 2 shows CIS scans for both peak A and peak B at different concentrations: in figure 2(*a*) the resonance character of peak A can clearly be seen in both samples, but the

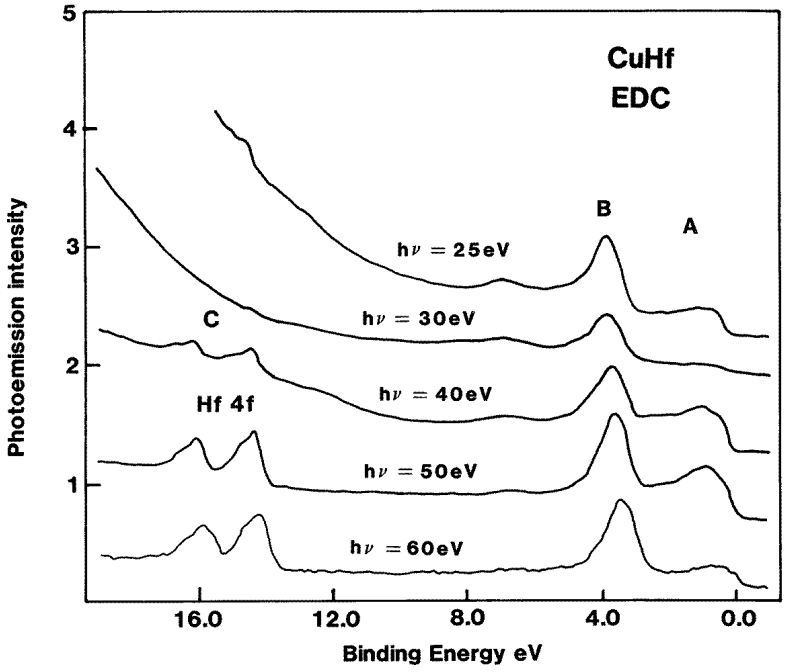

Figure 1. EDC curves of $Cu_{0.12}Hf_{0.88}$ for photon energies between 25 eV and 60 eV.

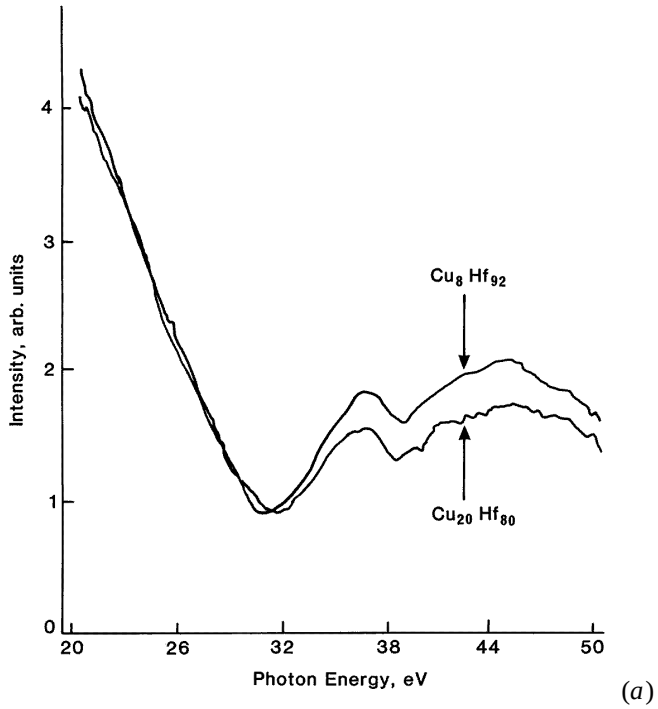

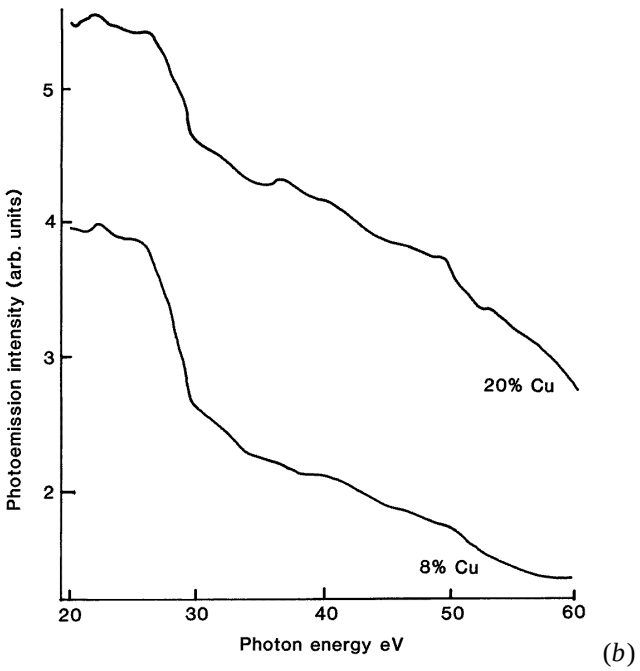

Figure 2. (*a*) CIS curves at a binding energy of 1 eV corresponding to peak A in figure 1 for two CuHf compositions. The resonance has a double-peaked structure. (*b*) Corresponding CIS curves at a binding energy of 3 eV corresponding to peak B in figure 1. No resonance can be seen, and the drop in intensity towards higher photon energy shows peak B to be predominantly Cu 3d in nature.

resonance is stronger in the sample with higher Hf content. In contrast peak B (figure 2(*b*)) shows no resonance but only a change of gradient in the decrease in photoemission cross-section with increasing photon energy. These results are consistent with peak A having strong Hf 5d character, while peak B is mainly associated with Cu 3d states, as inferred previously by Walker *et al* [8].

We can describe the resonant enhancement of the 5d partial cross-section of Hf as quasi-atomic $5p^6 5d^n \rightarrow 5p^5 5d^{n+1}$ transitions ($n \sim 2$–3) followed by direct recombination leading to a final state $5p^6 5d^{n-1}$, that of direct 5d photoionization: the interference between the two channels leads to a characteristic Fano profile. In this energy range the differential cross-sections for 5d-like photoemission will be higher than those predicted by Yeh [13] who considers only direct photoemission, while those of the free electron sp-like states have negligible cross-section (figure 1). The Hf resonance is double peaked due to spin–orbit interaction [8] and occurs at energies well above the 4p binding energy.

With the photoemission peaks at 14–16 eV unambiguously due to the Hf 4f levels and those at 3.5 eV mainly due to Cu 3d-like states as implied by the absence of resonance behaviour it is possible to glean more information about the conduction band states near the Fermi edge by comparing the intensities of peaks A, B and C as a function of composition. If the density of states near the Fermi edge were purely Hf 5d-like with no contribution from other states, then, at a particular photon energy, the ratio of intensities peak A (Hf 5d?)/peak C (Hf 4f) would be to first order independent of composition. In the same spirit, if x is the fractional composition of Cu in the alloy, the area of the Hf 4f peak should be proportional to $1 - x$ and the area of the Cu 3d peak to x. Hence a plot of y, the ratio of the intensities of peak C/peak B, should follow the relation

$$y = k(1 - x)/x = kx^{-1} - k \tag{1}$$

where k is a positive constant approximately proportional to the ratio of the appropriate Hf 4f to Cu 3d differential photoemission cross-sections. Hence a plot of y against the reciprocal of Cu concentration should give a straight line. On the other hand, if a particular feature (e.g. peak A) consists of a superposition of contributions from both Hf 5d and Cu 3d states then $z =$ peak A/peak B would take the form

$$z = [k_1(1 - x) + k_2 x]/x = (k_2 - k_1) + k_1 x^{-1} \tag{2}$$

where k_1 is approximately proportional to the ratio of the photoemission cross-sections of Hf 5d and Cu3d, while k_2 is related to the fractional Cu 3d character in peak A. By plotting z against the reciprocal of the Cu concentration, a straight line should still result, but there will be a residual value of z at $x = 1$. The arguments of course assume that hybridization leads to cross-sections which are superpositions of free atom cross-sections: this may not be wholly valid but such an analysis should give a first-order description of concentration and hybridization effects.

Figure 3 shows plots of Hf '4f'/Cu '3d' intensity for photon energies 35, 45 and 60 eV versus inverse Cu concentration $1/x$ and least-squares fitted lines giving equal weight to all points. Within these limitations the agreement with equation (1) is good, with the gradient increasing with photon energy as the 4f Hf cross-section steadily increases relative to that of Cu 3d. At $1/x = 1$, y shows only a very small value. These results give strong support to the view that peak B can be mainly associated with Cu 3d character.

Figure 4 shows a similar series of plots for the peak A/peak B ratio: a good straight-line fit is again possible but agreement with equation (1) is now somewhat poorer with a slightly larger z residue at $1/x = 1$ suggesting that one may require equation (2) or beyond to explain the behaviour, i.e. another component (Cu 3d?) besides Hf 5d may be contributing to the

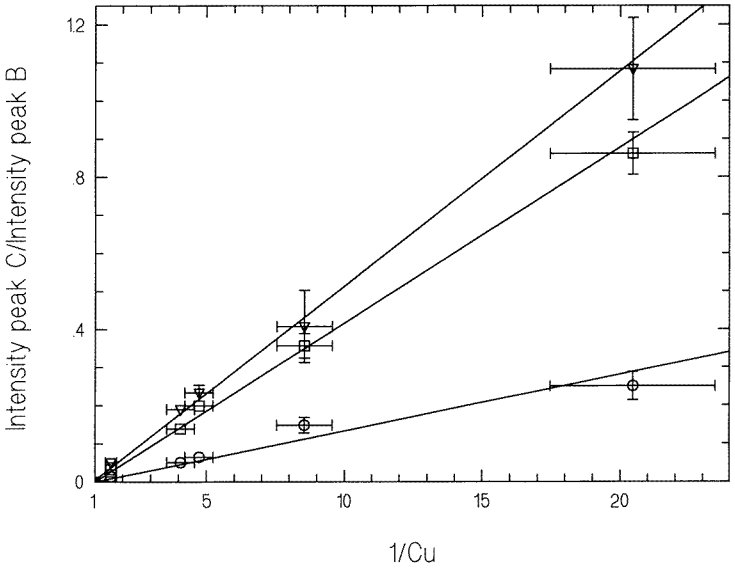

Figure 3. Ratio of 4f peak area to 3d peak area as a function of the reciprocal of the Cu composition ($1/x$) for photon energies of 35, 45 and 60 eV. In each case, the data can be closely described by equation (1) with the gradients increasing with increasing photon energy.

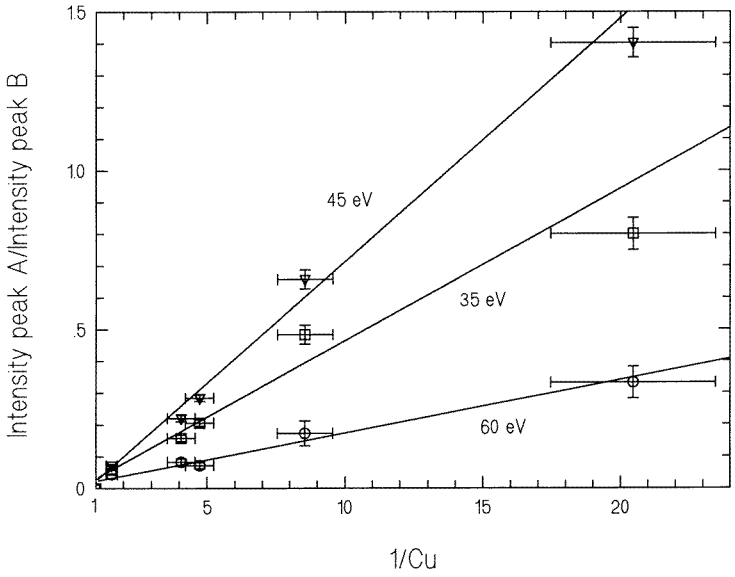

Figure 4. Ratio of 5d peak area to 3d peak area as a function of the reciprocal of the Cu composition ($1/x$) for photon energies of 35, 45 and 60 eV.

intensity of peak A. The gradients of the plots reflect the ratio of the Hf 5d/Cu 3d cross-sections which peaks at $h\nu = 45$ eV, and then declines as Hf 5d goes beyond resonance. The possible presence of Cu 3d character in the peak A binding energy region will be examined in greater detail in experiments at higher photon energy—see section 3.4.

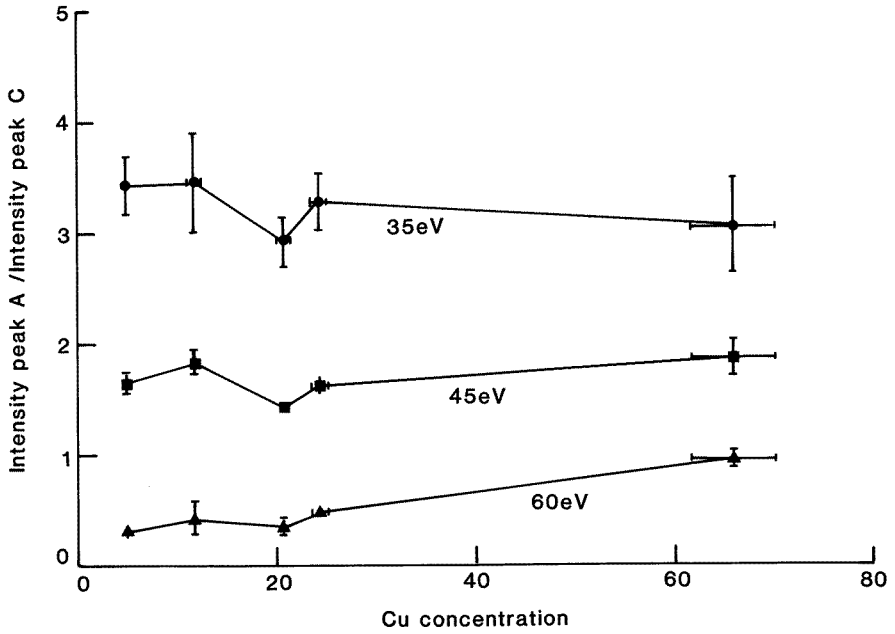

Figure 5. Ratio of 5d peak area to 4f peak area as a function of the percentage Cu composition for photon energies of 35, 45 and 60 eV.

Figure 5 shows the peak A/peak C intensity ratio plotted against Cu concentration for photon energies 35, 45 and 60 eV. If the valence band photoemission were purely Hf 5d in nature, then such a ratio (5d Hf/4f Hf) would be constant at all concentrations for a particular photon energy. At $h\nu = 35$ and 45 eV this is largely true apart from a dip in the ratio at around 20% Cu concentration. The effect was observed on a number of samples and on two separate runs several months apart, differing only slightly in position and intensity between comparable samples. *In situ* resistivity measurements and x-ray observations of CuHf films prepared under these conditions imply the development of a polycrystalline rather than an amorphous state beyond 80–85% Hf content and it is possible that at compositions close to this transition the $5p^5 5d^{n+1}$ excited state may be less localized, leading to a reduced probability of direct recombination into the photo-emission channel. At $h\nu = 60$ eV there is a slight increase in the intensity ratio with increasing copper concentration consistent with the possibility of increasing participation of Cu 3d states in the near-Fermi-level region as suggested in figure 4.

3.3. CuZr photoemission peak intensities—resonance region

Figure 6 shows the electron energy distribution for photoemission from $Cu_{0.3}Zr_{0.7}$ at $h\nu = 45$ eV, in the region of $4p^6 4d^n \rightarrow 4p^5 4d^{n+1}$ photoexcitation leading to resonance enhancement of the conduction band photoemission. Figure 7 gives the CIS scan for the same sample: this follows a similar pattern as CuHf with peak A displaying strong resonance well above the 4p ionization threshold at 29 eV, and peak B showing no resonance behaviour but having some gradient change in the resonance region. Unfortunately there is no weakly bound core peak adjacent to the conduction band that can be used for comparison as in the case of CuHf, but the relative intensities of peak B and peak A vary with composition and

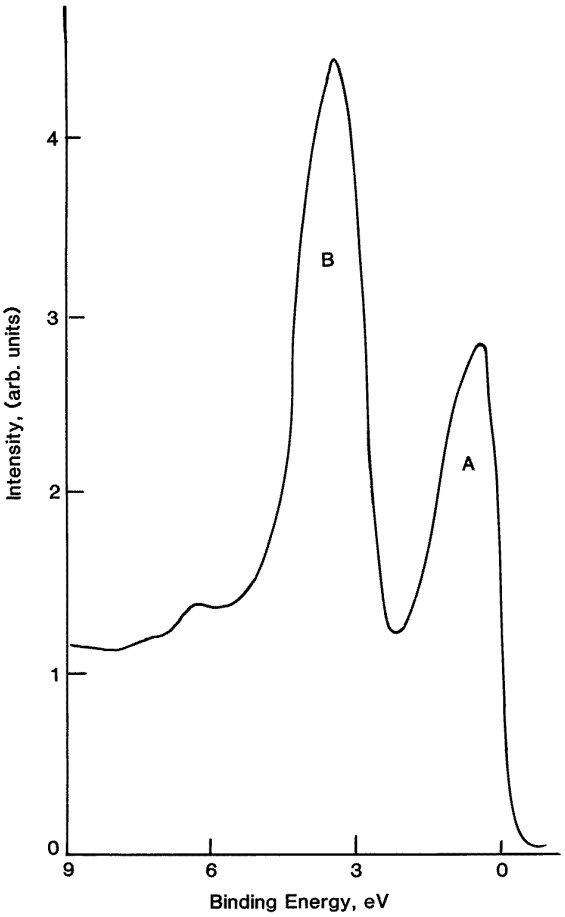

Figure 6. The electron energy distribution for photoemission from $Cu_{0.3}Zr_{0.7}$ at $h\nu = 45$ eV, i.e. in the region of the 4p→4d resonance.

energy in a manner qualitatively similar to CuHf. Figure 8 plots the photoelectron energy distribution curves for a range of Cu_xZr_{1-x} alloys at $h\nu = 50$ eV, a photon energy just beyond the 4p→4d resonance at which the intensity of peak A is already well reduced. At high Cu concentration ($x = 0.89$ and $x = 0.71$) the Cu 3d has a doublet structure similar to that in Cu metal, but at low concentration ($x = 0.46$) the band narrows, as in the case of Cu_xHf_{1-x}, due to reduced Cu 3d–Cu 3d overlap.

3.4. Photoemission—Cooper-minimum regions

In the photon energy region of np→nd excitation, photoemission below the Fermi edge is dominated by nd Hf or Zr resonant photoemission, but as the photon energy increases contributions from Cu 3d states begin to play a role. Indeed above $h\nu = 50$ eV there is a rapid reduction in the Hf (Zr) nd partial cross-sections due to the existence of Cooper minima [14] associated with nodes in the 4d/5d transition metal wavefunction. This is already apparent in the photoemission intensities at $h\nu = 50$–60 eV in CuZr—see figures 7 and 8.

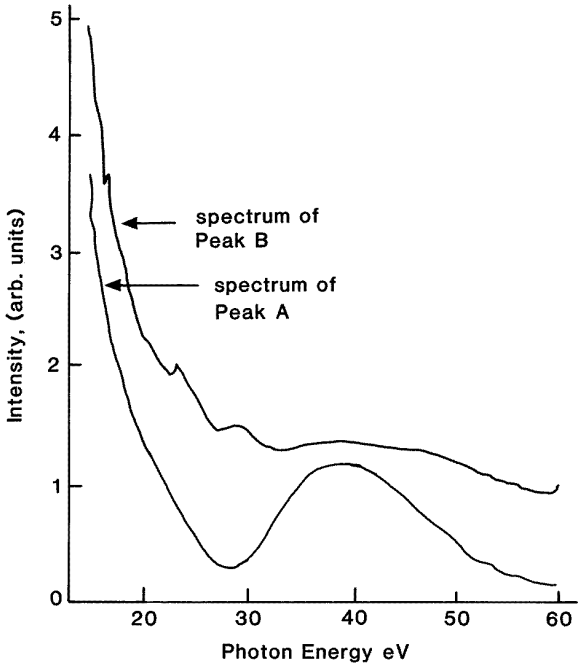

Figure 7. CIS for $Cu_{0.3}Zr_{0.7}$ at binding energies 1 eV (peak A) and 3 eV (peak B).

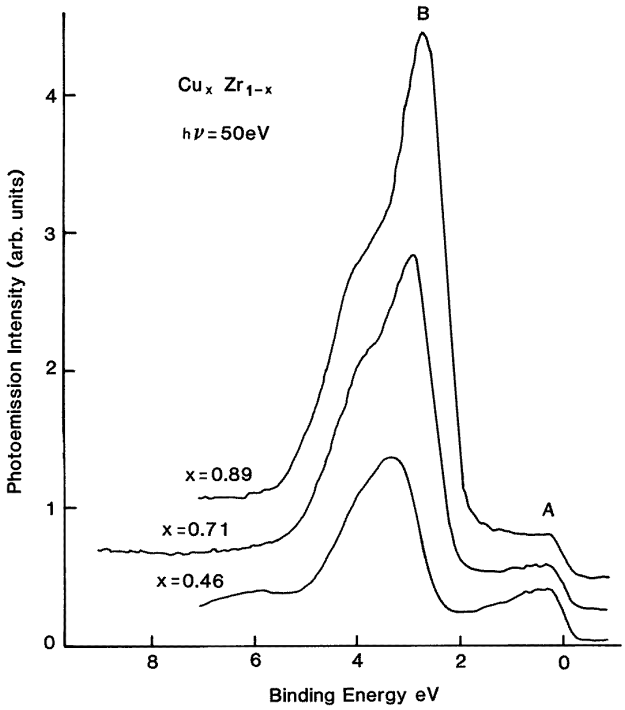

Figure 8. EDC curves for Cu_xZr_{1-x} at $h\nu = 50$ eV for $x = 0.89$, 0.71 and 0.46 as determined by EDX.

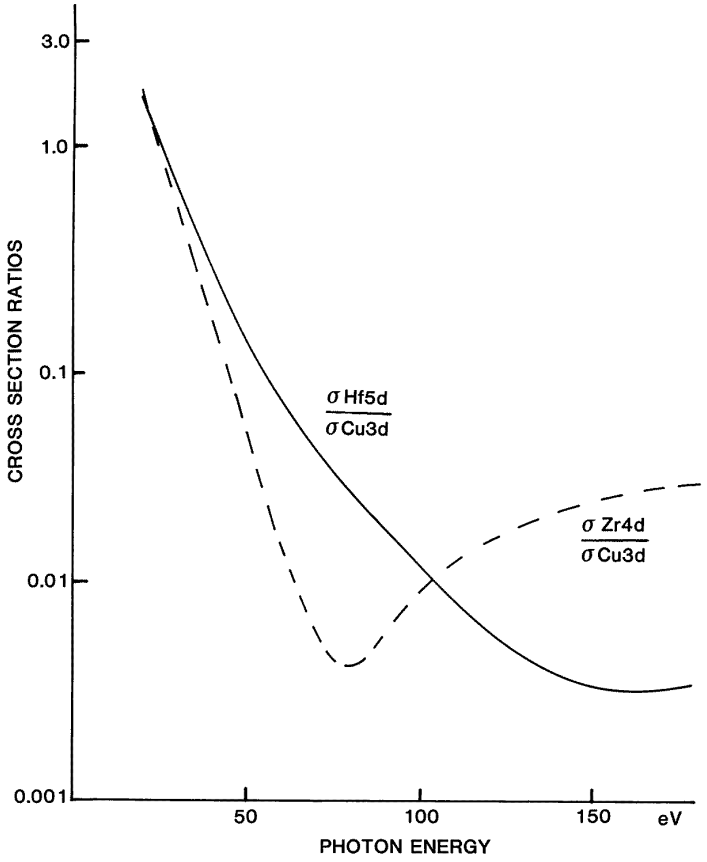

Figure 9. Theoretical estimates of the direct σ(Hf 5d)/σ(Cu 3d) and σ(Zr 4d)/σ(Cu 3d) photoionization cross-section ratios as a function of photon energy.

In free Hf and Zr atoms, Yeh [13] predicts a reduction in one-electron photoionization cross-section of more than two orders of magnitude between the maximum cross-section, which does not take account of the np$\rightarrow n$d resonances, and the Cooper minima at $h\nu \sim 80$ eV (Zr) and $h\nu \sim 180$ eV (Hf): figure 9 plots the estimated ratio of Hf 5d/Cu 3d and Zr 4d/Cu 3d cross-sections.

Station 6.1 was used to map the intensities of the shelf region near the Fermi edge (formerly peak A!) in relation to the area under the Cu 3d band for both Cu Hf and polycrystalline Cu. Figure 10 compares the conduction band photoemission at $h\nu = 160$ eV, i.e. close to the CuHf Cooper minimum, of Cu metal and amorphous $Cu_{0.25}Hf_{0.75}$. Note how the Cu 3d band narrows into a single peak closer in character to a virtual bound state on forming the alloy as the Cu 3d–Cu 3d overlap is reduced. The differing 3d band breadths in the two systems makes comparison difficult, and the following scheme was adopted. The shelf area within 1.5 eV of the Fermi edge and the area under the Cu 3d peak or peaks were measured with a smooth background removed in the latter case. The ratio of the areas was then plotted against photon energy (figure 11): this does not take account of the full area of the peak A region in the alloys and as a result the area ratios at low photon energy (<60 eV) are less than previously estimated for alloys of similar composition (figure 4). However, the

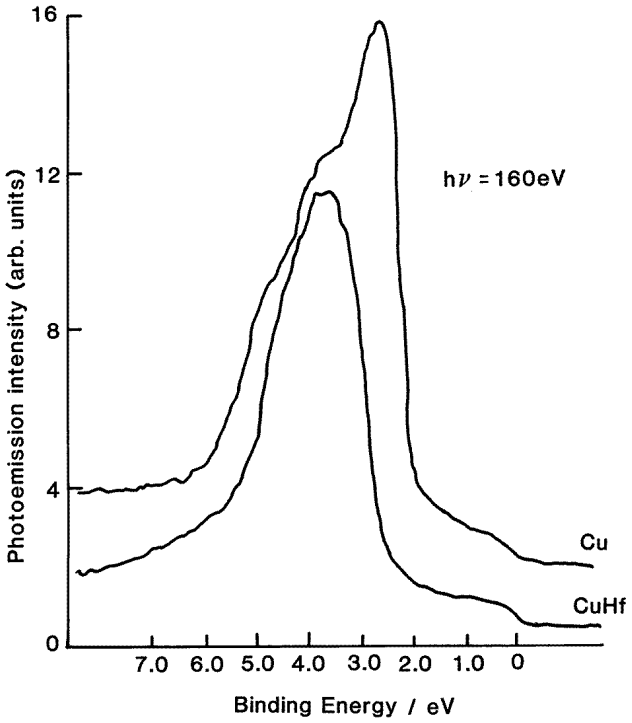

Figure 10. Comparison of the electron energy distributions for $Cu_{0.25}Hf_{0.75}$ and Cu metal at photon energy $h\nu = 160$ eV.

fact that the area ratio can be consistently applied for the two systems suggests that the plot gives a good indication of how the relative intensities in the two regions vary with photon energy. In CuHf the ratio starts high due to the near resonant Hf 5d contribution but falls off quickly until above $h\nu = 100$ eV 'non-pure 5d Hf' states will make the predominant contribution to the cross-section. The shelf/peak ratio in Cu is much lower than in CuHf at low photon energy and declines to a shallow minimum around 100 eV before rising slightly. We believe that this effect is likely to be an artefact associated with the somewhat arbitrary area partitioning procedure. The ratio is, however, in good agreement with that inferred from the article by Zhang *et al* [15] at $h\nu = 80$ eV.In spite of these limitations two features emerge:

(i) the shelf to Cu 3d peak ratio is greater than that of Cu in the Hf 5d Cooper-minimum region, and
(ii) the reduction in intensity in the near-Fermi-energy region with increasing photon energy is much less than that predicted for Hf 5d atomic photoemission.

That the Cooper minima in solid state environments are often much shallower than in the free atom is now well established—see for example the articles by Cole *et al* [16], Oh and Nahm [17], D'Addato *et al* [18] and Liddiard *et al* [19]. In Ag metal [16] the reduction in the depth of the Cooper minimum can be attributed to hybridization of Ag 4d wavefunctions with those of neighbouring atoms, and in $Au_{95}Pd_5$ [17] there is also strong evidence of distortion of the Pd 4d wavefunctions. While such distortion effects will be important here it is possible that the suppression of photoionization intensity in the Cooper-minimum region

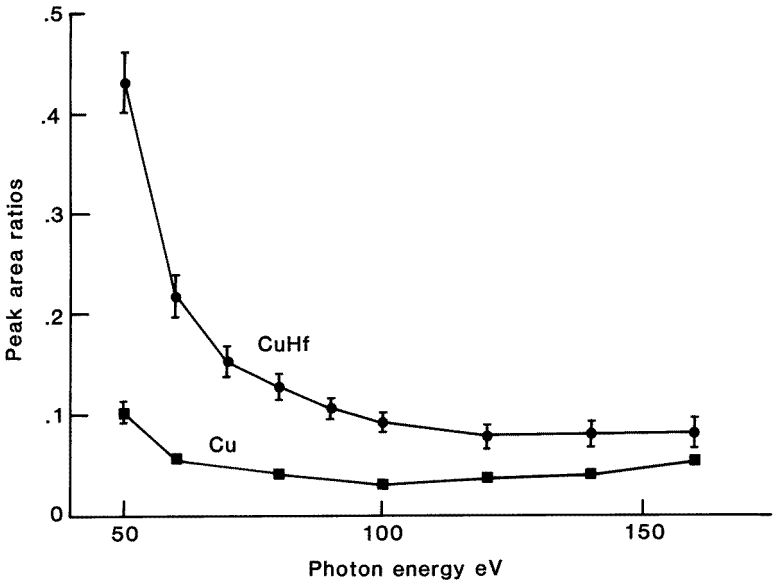

Figure 11. The variation of the ratio of the near-Fermi-level shelf area to the 'Cu 3d' peak area in Cu metal and $Cu_{0.25}Hf_{0.75}$ with photon energy.

will be sufficient for the photoionization intensity to be described to first order by the simple superposition model of Zhang *et al* [15]

$$I(h\nu,\ \mathrm{BE}) = C(h\nu)[\sigma_{Cu}(h\nu)D_{Cu}(\mathrm{BE})/Z_{Cu} + \sigma_{Hf(Zr)}(h\nu)D_{Hf(Zr)}(\mathrm{BE})/\mathrm{Z}_{Hf(Zr)}] \tag{3}$$

where D_i(BE) is the partial d density of states of the element i at binding energy BE constrained by the relation

$$\sum_i D_i(\mathrm{BE})\,\Delta\mathrm{BE}_i = N_i Z_i \tag{4}$$

where N_i and Z_i are respectively the concentration and number of d electrons of the ith element; $C(h\nu)$ takes account of instrumental response effects. Such a model was implicit in our intensity analysis in the resonance region. Assuming that the Cooper minimum (albeit in attenuated form) is sufficiently deep that $\sigma_{Cu}(h\nu)/Z_{Cu} \gg \sigma_{Hf}(h\nu)/Z_{Hf}$ above $h\nu = 100$ eV, the 3d copper partial density of states would contribute about 0.25 electrons in the near-shelf region compared to 1.5 Hf electrons per formula unit overall (assuming $Z_{Hf\,5d} = 2$), i.e. in and beyond the region 1.5 eV below E_F. On these assumptions about 15% of the partial density of states in the peak A region has Cu 3d rather than Hf 5d character in $Cu_{0.25}Hf_{0.75}$. However the effect may also be associated with Hf 5d–Hf 5d and Hf 5d–Cu 3d wavefunction overlap leading to differing distortion of the wavefunctions at the edge of the atom as in the case of pure Ag and its alloys [16] rather than direct contributions from Cu 3d partial density of states near the Fermi edge. It is of interest to examine the phenomenon for Cu_xZr_{1-x} at a range of concentrations, with the Zr Cooper minimum occurring at much lower energy.

Figure 12 shows the corresponding peak A/peak B ratios for Cu_xZr_{1-x} as a function of photon energy from $h\nu = 50$ eV up to 180 eV. Cooper minima are apparent at photon energies just below $h\nu = 100$ eV but somewhat above the energy predicted by Yeh [13]—see figure 9. Furthermore the ratio of the intensity at the Cooper minima to that at $h\nu = 50$ eV

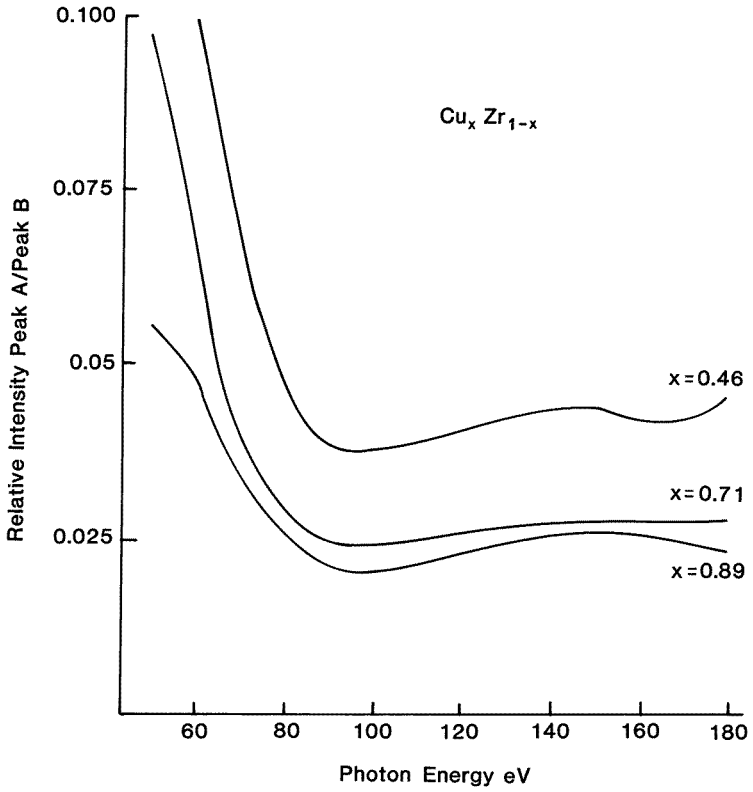

Figure 12. The ratio of the intensities of peak A to peak B for the samples of figure 8 in the photon energy range 50–180 eV.

is much higher than its value in the free atom, and the recovery in peak ratio beyond the minimum is much less than that predicted for atomic Zr. In Cu_xZr_{1-x} with $x = 0.89$ and 0.71 the fact that the Cooper-minimum profiles are very shallow on the high-energy side supports the view that the observed peak A photoemission intensity beyond 100 eV is predominantly due to Cu 3d-like states. In addition the magnitude of the peak A/peak B ratio in that region is comparable to that for Cu metal (figure 10) so there is little evidence of enhanced Cu 3d character near the Fermi edge. At higher Zr concentration ($x = 0.46$) with higher probability of Zr–Zr nearest neighbours the increase in intensity beyond $h\nu = 100$ eV suggests that Zr 4d states may now be contributing significantly to the emission with the depth of the Cooper minimum reduced at least partly through like atom d overlap as in the emission from Ag metal [16]. Overall evidence suggests that photoemission from the near-Fermi-level region of Cu Hf and Cu Zr alloys shows both residual Cu 3d-like character and modified Cooper minimum behaviour of Zr and Hf. It is probable that the number of like, as opposed to unlike, atomic neighbours is more significant in determining the relative spectral intensities than the existence of an amorphous rather than polycrystalline environment.

Finally detailed studies of the shape of the Fermi edge region were attempted both at low photon energy ($h\nu \sim 40$ eV) and higher photon energies with the objective of identifying Fermi edge anomalies associated with strong correlation effects in the amorphous alloy. The increase in Fermi edge breadth with increasing photon energy was shown to be consistent

with the variation of the electron spectrometer energy resolution with increasing kinetic energy, and, as in the work of Zhang *et al* [15] and Stadnik *et al* [20] looking for the pseudo-gap in $Al_{65}Cu_{20}Os_{15}$, much higher energy resolution is required to address such questions.

4. Discussion

The dual tools of resonant photoemission and Cooper minima in photoionization cross-sections have been used to give insights into hybridization in amorphous Cu_xHf_{1-x} and Cu_xZr_{1-x} alloys with particular emphasis on the relative intensities of the two main photoemission peaks from the conduction band, one nominally associated with Cu 3d states, the other with *n*d states of the transition metals. The resonances in Hf and Zr are very intense, totally dominating direct photoemission close to E_F, and much stronger than is observed in the middle of the transition metal series, e.g. in the recent work of Stadnik *et al* [20] and Zhang *et al* [15] on the Ru and Os resonances in icosahedral alloys $Al_{65}Cu_{20}Ru_{15}$ and $Al_{65}Cu_{20}Os_{15}$, where the Fano profiles exhibit characteristic dips prior to the resonance as observed in FeZr [7], and in the Mn resonance in Cu_2MnAl [21]. In CuHf the CIS plot shows clearly spin–orbit splitting in the resonance profile consistent with the results on electron excited autoionization of Sanz [22], while in CuZr the spin–orbit effects are unresolved, results similar to those obtained on ZrO_2 by Sanz *et al* [23].

The intensities of the resonances suggest that the observed peaks in the density of states immediately below the Fermi edge are Hf (Zr) 5d (4d) dominated, but more detailed analysis of both the resonance and the Cooper-minimum regions gives support to the view that there is substantial Cu 3d hybridization in the wavefunctions of states in that region. A simple superposition of atomic cross-sections model has been applied to account for the concentration dependence of the relative intensities of the two peaks in the conduction band and in the case of CuHf the conveniently placed Hf 4f core peaks below. At higher binding energy the gradient change in the CIS curve in the region of the Hf and Zr resonances suggests that there is some influence from the higher-series transition metal. In the case of the peak near the Fermi edge there is evidence for hybridization between Hf (Zr) 5d (4d) and Cu 3d wavefunctions both in the intensity plots at photon energies around the resonance region and in the Hf/Zr Cooper-minimum region where residual Cu character in the states is exposed, especially for low Zr concentrations in Cu_xZr_{1-x}. Approximate estimates of the hybrid character of the states near the Fermi level have been derived but these should be treated with caution. It is clear from the work of Cole *et al* on Ag [16] that distortion of atomic wavefunctions in the overlap region can have profound effects on quasi-atomic cross-sections, implying that subtracting photoemission profiles at different photon energies from one another may give subtler information than simple atomic superposition models would suggest. This seems likely to be important at lower Cu concentrations where Hf–Hf and Zr–Zr overlap dominate.

It is useful to compare these estimates with the partial densities of states for amorphous CuZr calculated by Fairlie *et al* [24]. DOS calculations on $Zr_{0.7}$ with $Cu_{0.3}$, $Ni_{0.3}$ and $Fe_{0.3}$ confirm the presence of two well separated d bands. In FeZr the partial densities of states on both sites are split into bonding and anti-bonding bands with the bonding Fe–Zr band equally distributed over both sites, while the anti-bonding bands of Fe and Zr are well separated and in the case of Zr partially filled. By contrast in CuZr the bonding–anti-bonding splitting of the Cu decreases and the Cu partial state density moves to higher binding energy to form the relatively sharp quasi-filled Cu 3d band observed here. Fairlie *et al* [24] predict a small Zr component within the bonding part, a result consistent with the gradient change found in

the CIS spectrum within the Cu 3d band (figure 7). The theoretically predicted tail of Cu 3d states in the near-Fermi region is somewhat less prominent than implied by the Cu partial density of states inferred by Zhang *et al* [15] on the icosahedral alloy $Al_{65}Cu_{20}Os_{15}$, where again Cu bonds to a lower-transition element, and in this work on Cu_xZr_{1-x} and Cu_xHf_{1-x} if a simple superposition model is assumed. However, modification of the wavefunctions in the overlap region may be controlling the photoemission matrix elements in a manner not inconsistent with the predictions of Fairlie *et al* [24].

5. Summary

A combination of resonant photoemission and Cooper minima in atomic cross-sections has been exploited to study the conduction band densities of states of Cu_xHf_{1-x} and Cu_xZr_{1-x} amorphous alloys. The conduction bands have a basic two-peak structure with a higher-binding-energy peak which is Cu 3d-like in character and the peak near the Fermi level dominated by *n*d-like states which, however, exhibit much weaker Cooper minima than is predicted for the free atom. This gives evidence for substantial hybridization between Cu and Hf/Zr d states albeit on a level much weaker than in alloys such as FeZr where both constituents have open d shells.

Acknowledgments

We wish to thank EPSRC for financial support, Dave Teehan and Paul Bailey for station support at Daresbury, and John Turton for technical backup. One of the referees is acknowledged for constructive suggestions in the presentation of the manuscript.

References

[1] Howson M A and Greig D 1986 *J. Phys. F: Met. Phys.* **16** 989
[2] Howson M A and Gallagher B L 1988 *Phys. Lett.* **170** 265
[3] Oelhafen P 1983 *Glassy Metals II* ed H Beck and H-J Guentherodt (Berlin: Springer) p 283
[4] Oelhafen P, Hauser E, Guentherodt H-J and Bannerman K H J 1979 *Phys. Rev. Lett.* **43** 1134
[5] Amamon A and Krill G 1978 *Solid State Commun.* **28** 957
[6] Greig D, Gallagher B L, Howson M A, Law D S-L, Norman D and Quinn F M 1988 *Mater. Sci. Eng.* **99** 265
[7] Walker C G H, Hucknall P K, Greig D, Walker M J, Turton J, Matthew J A D and Norman D 1992 *Solid State Commun.* **82** 573
[8] Walker C G H, Hucknall P K, Matthew J A D, Norman D, Greig D, Walker M J and Turton J 1992 *Surf. Sci.* **269/270** 610
[9] Morton S A, Turton J and Greig D 1995 *Rev. Sci. Instrum.* **66** 3917
[10] Davis L E, MacDonald N C, Palmberg P W, Riach G E and Weber R E 1976 *Handbook of Auger Electron Spectroscopy* 2nd edn (Eden Prairie, MN: Perkin Elmer Corp. Physical Electronics Division)
[11] Walker C G H, Peacock D C, Prutton M and El Gomati M M 1988 *Surf. Interface Anal.* **11** 266
[12] Hucknall P K, Walker C G H, Greig D, Matthew J A D, Norman D and Turton J 1992 *Surf. Interface Anal.* **19** 23
[13] Yeh J-J 1993 *Atomic Calculation of Photoionisation Cross Sections and Asymmetry Parameters* (London: Gordon and Breach)
[14] Cooper J W 1962 *Phys. Rev.* **128** 681
[15] Zhang G W, Standik Z M, Tsai A-P, Inouie A and Miyazaki T 1995 *Z. Phys.* B **97** 439
[16] Cole R J, Evans J A, Duò L, Laine A D, Fowles P S, Weightman P, Mondio G and Norman D 1992 *Phys. Rev.* B **46** 3747
[17] Oh S-J and Nahm T-Uh 1996 *J. Electron Spectrosc. Relat. Phenom.* **78** 43
[18] D'Addato S, Brooks N J, Thornton J M C, Unsworth P, Weightman P, Duò L and Sancrotti M 1996 *J. Phys.: Condens. Matter* **8** 1413

[19] Liddiard A J, Brown D, Crapper M D, Petty M, Smith J G, Telling N D, Bedwell K H, Flannery L B and Skull P A 1996 *J. Phys.: Condens. Matter* **8** 3955
[20] Stadnik Z M, Zhang G W, Tsai A-P and Inouie A 1994 *J. Phys.: Condens. Matter* **6** 6885
[21] Brown D, Crapper M D, Bedwell K H, Flannery L B, Petty M and Skull P A 1996 *J. Phys.: Condens. Matter* **8** 5941
[22] Sanz J M 1991 *Surf. Sci.* **251/252** 204
[23] Sanz J M, Gonzalezelipe A R, Fernandez A, Leinen D, Galan L, Stampfl A and Bradshaw A M 1994 *Surf. Sci.* **309** 848
[24] Fairlie R H, Temmerman W M and Gyorffy B L 1982 *J. Phys. F: Met. Phys.* **12** 1641